Taylor & Francis
Taylor & Francis Group

Lacunarity analysis to determine optimum extents for sample-based spatial information extraction from high-resolution forest imagery

C. R. BUTSON and D. J. KING*

Department of Geography and Environmental Studies, Carleton University,
1125 Colonel By Drive, Ottawa, Ontario K1S 5B6, Canada

Lacunarity analysis was evaluated as a means to determine multiple pattern scales that are inherent in high-resolution imagery of forests and to specify an optimal spatial extent for spatial image information extraction. A series of 0.5 m pixel images of temperate hardwood and mixed boreal forests were analysed using lacunarity distributions calculated for spatial extents ranging from 7 m to 40 m. The optimal extent was taken as that which displayed the greatest number of distinct pattern scales. For the temperate hardwood forest dataset, 12–14 m extents were found to be optimal, detecting three pattern scales. For the boreal forest dataset, optimal extents were 14–18 m for five of six plots, detecting two or three pattern scales in each plot. The detected pattern scales ranged from 8 m to 14 m and showed some correspondence to tree crown size, but also responded to clusters of understorey and overstorey trees or to partially exposed tree crowns. The method can aid in determination of the sample extent that best captures the pattern scales present in the imagery. More generally, it can be useful in exploratory analysis of any spatial data for which the fundamental patterns are not known.

1. Introduction

Measurement of the patterns of objects within geo-spatial data and the scales at which they occur can aid in development of an understanding of the spatial variation and of object relations within the data. Spatial patterns dominant in forests can be characterized (ideally) as dispersed, random or clustered (Upton and Fingleton 1985) with these characteristics being scale dependent (Dale 2000). Trees in a plantation may exhibit a regular pattern with a uniform spatial distribution. They mature at the same time and their even spacing ensures consistent structural characteristics over the occupied space. In more natural forests, there is typically no dominant trend or spatial pattern. The arrangement of trees often follows a Poisson distribution (Nigh 1997), where the probability of tree occurrence in space can be modelled as a random discrete event, given knowledge of the average rate of occurrence (McGrew and Monroe 1993, Taylor 1997). A clustered forest exists when there is autocorrelation present in the spatial location of trees (Stiteler and Patil 1971). At the landscape scale, spatially fragmented forests are clumped patches of vegetation within an agriculture or developed environment. At

---

*Corresponding author. Email: doug_king@carleton.ca

the patch level, clumping can occur in tree locations due to environmental-site characteristics, stress or damage, and forest management activities (Zoladeski and Maycock 1990).

Quantifying the spatial characteristics of the forest canopy using remote sensing data can facilitate data exploration and understanding of spatial processes. Such spatial data measured at multiple scales could extend analysis from relatively localized study areas to more broad-scale landscapes. Since much of remote sensing research is related to the scale of interest (Woodcock and Strahler 1987, Marceau *et al*. 1994, Hay *et al.* 2003), measuring data characteristics at a variety of scales can allow relations between variables at one scale to be linked to similar variables at other scales. By modelling forest spatial pattern over several scales it is possible to identify dominant scaling regions or *natural scales* (Hay *et al.* 2003) in the data. These regions often reflect the size of inherent objects in ground units. Since it is widely recognized that natural systems operate over many scales (Mandelbrot 1983), fractal and other multi-scale spatial analysis methods are currently being applied in forestry (De Cola 1989), geology (Sim *et al.* 1999) and landscape ecology (With and King 1999) to characterize surface patterns at a wide range of spatial resolutions and to describe how the identified patterns change with observed scale. In this research, lacunarity, as a multi-scale measure of spatial pattern (Plotnick *et al.* 1996, Dale 2000, McIntyre and Wiens 2000) was analysed in high-resolution forest image data to determine pattern scales, their relations to forest characteristics, and the optimal spatial extent required to capture the most distinct of these patterns. A detailed definition and description of lacunarity analysis is given in the Background section below.

Previous research has found lacunarity measurements to be useful for quantifying the scale of spatial pattern in real and simulated imagery. For example, in landscape ecology, Dale (2000) compared the properties of lacunarity analysis of one-dimensional data to local variance techniques in the context of two themes: (i) pattern as points in space, and (ii) pattern as the arrangement of patches and gaps. The results showed that lacunarity analysis identified multiple pattern scales in the data and that lacunarity differed for complementary patterns (ones (1s) and zeros (0s) reversed in binary data), a characteristic seen as potentially advantageous for landscape structure analysis. McIntyre and Wiens (2000) found lacunarity analysis to be useful in detecting non-randomness and scale dependence of animal movements in relation to landscape patterns while With and King (1999), in simulation modelling, linked dispersal success to lacunarity thresholds of landscape gap structure. In remote sensing, Sun and Ranson (1998) studied the effects of natural disturbance and forest management practices on the lacunarity of forest patterns in binarized radar imagery. Henebry and Kux (1995) evaluated seasonal differences in surface land cover dynamics in the Brazilian Pantanal using lacunarity analysis of European Remote Sensing Satellite (ERS)-1 Synthetic Aperture Radar (SAR) data. Weishampel *et al.* (1998), using lacunarity analysis of Landsat Multi-spectral Scanner (MSS) imagery, found differences in clumping (non-randomness) of Peruvian rainforest patches between the 1970s and 1980s, and linked them to changes in the nature of forest harvesting activities. More generally, Plotnick *et al.* (1996) demonstrated the flexibility of lacunarity analysis for use with many spatial pattern datasets. For example, analysis of γ-ray peaks from well logs showed them to be far more clustered at all scales than predicted from a random distribution.

1.1 *Objectives*

The goal of this research was to determine optimal spatial extents for sample-based analysis of forest structure using high-resolution remotely sensed imagery. The optimal extent is assumed to be the smallest area that captures the maximum amount of information content in the remotely sensed image patterns. Lacunarity analysis was implemented using imagery from two sites: one in the boreal forest, the other in a temperate hardwood forest. Specific objectives were:

(1) develop an algorithm to generate lacunarity curves and curves of its first derivative (spatial change in lacunarity) from a series of sample moving windows of varying sizes (extents), i.e. the gliding box method of Allain and Cloitre (1991) as recommended by Plotnick *et al.* (1996);
(2) interpret the resulting first derivative curves to determine spatial extents that capture the greatest number of pattern scales; and
(3) compare the measured pattern scales with tree crown dimensions measured in the field.

2. Background

The following provides a brief overview of the aspects of lacunarity relevant to this study. Lacunarity was originally introduced to measure the deviation of a fractal from translational invariance (Gefen *et al*. 1983) since some fractals were found to have the same dimension for visually different textures (Mandelbrot 1983). It represents the pre-factor in the general fractal power-law equation, where the exponent is the fractal dimension (**D**) (Henebry and Kux 1995). This is expressed in equation (1),

$$F(x) = \lambda(x)^{(\boldsymbol{D} - E)} \tag{1}$$

where $F(x)$ is the function, $\lambda(x)$ represents the lacunarity, $\boldsymbol{D}$ is the fractal dimension, and E is the Euclidean dimension. The lacunarity parameter (λ) describes the degree of heterogeneity of the fractal set. In a true fractal set, when $\lambda \to 1$, the variation in gap size is minimal and the pattern is self-similar. Self-similarity in a pattern refers to a fractal dataset that looks the same (homogeneous) across all observable scales. As $\lambda \to \infty$, a wide range of gap sizes is evident in the structure of the fractal producing a visually different texture. Thus, the concept and formulation of lacunarity arose from the problem of differentiating two objects defined by the same fractal dimension but presenting visually different textural patterns.

For binary images, lacunarity describes the distribution of 1s and 0s in the pattern and thus can be considered as a type of texture measure (Sun and Ranson 1998). Since lacunarity is a measure of gap pattern and size, the objects of interest are the gaps or holes in the pattern. For example, a map containing all 1s would be homogeneously occupied no matter what box size was used. If the same analysis were done on a map containing all 0s, the resultant lacunarity would approach infinity, as there are an infinite number of gap sizes inherent in the scene. Hence, in lacunarity analysis of a binary spatial pattern, the objects of interest should have a value of 0 and the background pattern a value of 1 (digital number, DN).

There are several proposed methods to measure lacunarity from a spatial dataset. The most common uses equation (2) to describe lacunarity (λ) as a function of the

box (window) size (*r*) from which the data are extracted (Allain and Cloitre 1991, Henebry and Kux 1995).

$$\lambda(r) = 1 + \text{variance} \Big/ (\text{mean})^2 \qquad (2)$$

This equation is derived from the first and second moments of the mean probability distribution function calculated at the specified box size. The mean value is a weighted average mass for the given box size used in the calculation. The variance is weighted based on the mass values measured for each box size. The basic assumptions of this technique are discussed thoroughly in Plotnick *et al.* (1993).

To measure lacunarity in a two-dimensional binary raster image, a gliding box (moving window) with size ($r \times r$) is translated through the data. At each cell location, the box mass (*M*) at a given position is determined as the total number of active sites (sites with a value of 1). Once the box has passed through the whole image, the frequency distribution [*n*(*M*,*r*)] is calculated from all box masses (*M*), and the corresponding probability distribution function [*Q*(*M*,*r*)] is derived by dividing *n*(*M*,*r*) by the number of cells processed (the number of box positions). The sum of each *M**Q(*M*,*r*) derives the mean probability distribution function and the sum of M^2*Q(*M*,*r*) derives the variance probability distribution function. Substituting these into (2) gives equation (3).

$$\lambda(r) = 1 + M^2 Q(M, r) \Big/ [MQ(M, r)]^2 \qquad (3)$$

The mean and variance represent the mass statistics measured for each box size. A double-log curve of lacunarity versus box size is plotted to show the spatial response function identifying (i) the change in spatial pattern across scales, and (ii) scales of pattern depicted in the image (Elkie and Rempel 2001). The shape of the response function depends only on the aggregation of objects within a given spatial pattern (Plotnick *et al.* 1993).

For the objectives of this research, only the relative shape of the lacunarity curve was of concern as it reflects the inherent spatial pattern and pattern fluctuations with reference to the box size range. Changes in absolute lacunarity values with respect to variable-sized spatial extents were not analysed. As shown in figure 1, the lacunarity curve is a graphical representation of the scale-dependent spatial non-stationarity in a dataset (Henebry and Kux 1995). A lacunarity function derived for a random pattern (figure 1(*a*)) shows a rapid decay with increasing box size (figure 1(*c*)), whereas a clumped pattern, such as the one in figure 1(*b*), produces a lacunarity function that declines more gradually to an inflection point, which approximates the average pattern or object scale in the data. In high-resolution forest imagery, this inflection point may be indicative of the average tree crown size. After the inflection point, the function shows a swift decay characterized by a more homogeneous pattern at larger box sizes. Both random and clumped patterns reach a lacunarity of 1.0 (ln λ=0.0) at large box sizes as they become homogeneous (McIntyre and Wiens 2000) with respect to the observation scale. More representations of simulated forest patterns and associated lacunarity curves, such as those of figure 1, are given in Sun and Ranson (1998).

To analyse the fluctuation points in the lacunarity function with a greater degree of certainty, the first derivative of the curve may be plotted against the box size (Dale 2000). As shown in figure 1(*d*), the lacunarity slope curve for a random spatial
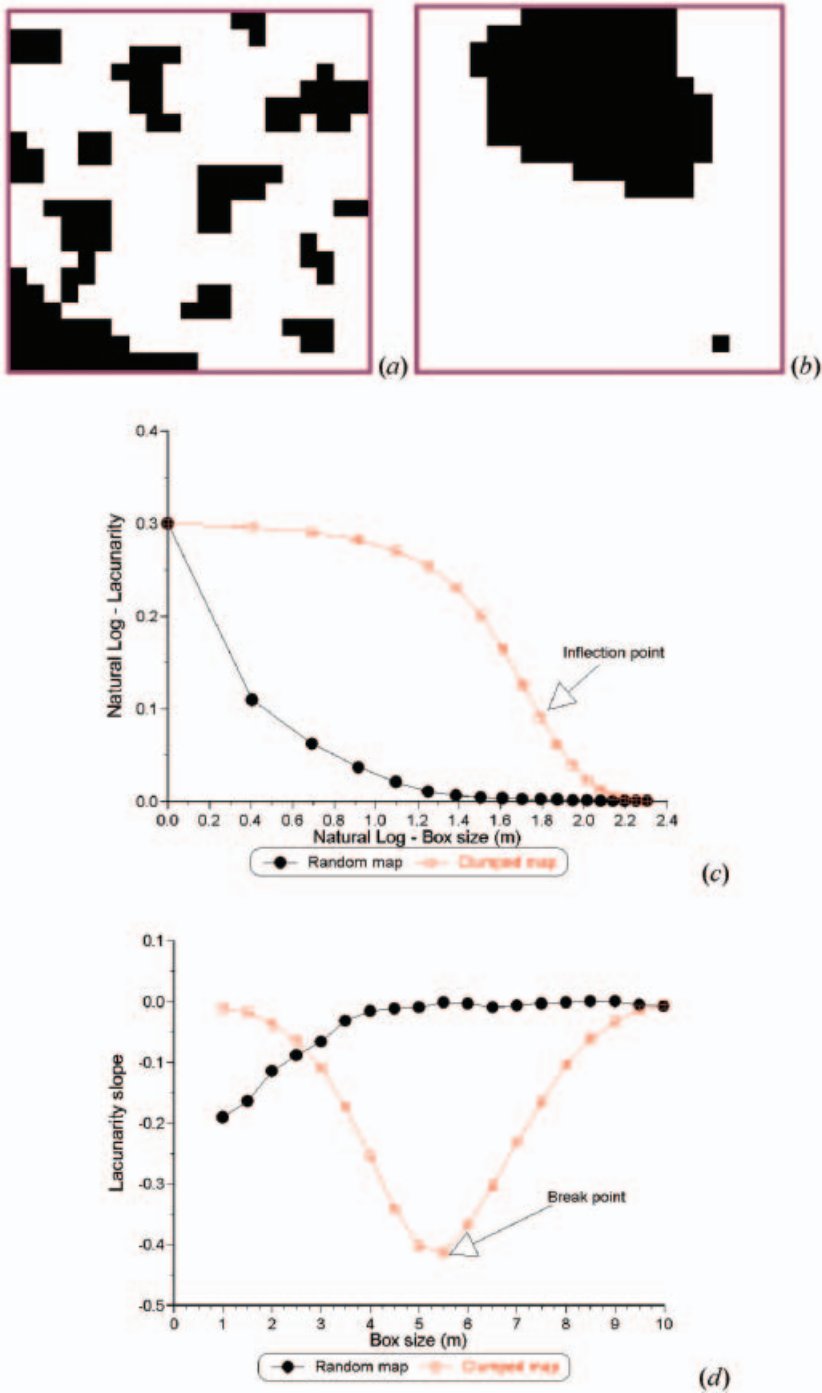
Figure 1. Example of (*a*) random map, (*b*) clumped map, (*c*) lacunarity function and (*d*) lacunarity slope function. Black is zero (0) and white is one (1). Original images were 21×21 pixels but have been expanded for presentation.

pattern begins with negative slopes that increase consistently throughout the curve. The curve plotted for the clumped pattern starts at a relatively modest negative slope, decays to the steepest slope at the break point (6 m), which corresponds to the inflection point in figure 1(*c*), and then increases towards 0 at larger box sizes. The trough width exhibited by the lacunarity slope curve indicates the rate of change in object sizes over the range of measured box sizes. A narrow trough indicates discrete break points in the pattern, whereas a wider trough reveals a more continuous change in object sizes. In this case, the object in the clumped pattern is irregular in shape and the deviation around the break point represents a more gradual change of object sizes. At such break points in the first derivative lacunarity curve, the spatial distribution and size of objects (the pattern) in a remote sensing scene are captured. The smallest extent that captures the greatest number of such pattern scales was taken as optimal for sample-based spatial image information extraction under the given image–forest conditions.

3.   Materials and methods

3.1   *Study sites, field data and airborne imagery*

Two distinctly different sites were used to study forest canopy spatial patterns characterized in different eco-regions. Dataset 1, in the Gatineau Park, Quebec, about 15 km north-west of the city of Ottawa, was an unmanaged temperate hardwood forest typical of the Great Lakes–St Lawrence forest region. Dataset 2 was 10 km north-west of Timmins, Ontario, in the boreal forest region. Both study sites have been described in previous papers as they are part of a larger research programme in forest structure, health and composition analysis in stressed environments using remote sensing (e.g. King 2002, Lévesque and King 2003, Seed and King 2003, Cosmopoulos and King 2004, King *et al.* 2005).

3.1.1   Dataset 1. Dataset 1 consisted of two 100 m × 50 m forest sample plots (plots 701 and 702) that are part of a system of permanent plots throughout Quebec maintained by the Quebec Ministry of Natural Resources (QMNR). The species composition of the plots and the surrounding forests in the region is dominated by overstorey sugar maple (*Acer sacc-arum*) with some basswood (*Tilia americana*), while the forest understorey consists of white ash (*Fraxinus americana*), ironwood (*Ostrya virginiana*), beech (*Fagus grandifolia*) and white birch (*Betula papyrifera*). Both plots were similar in species composition although one was situated in a well-drained elevated portion of the forest while the other was located in lower land with poorer drainage. The forest structure at the sites had been impacted by a severe ice storm in 1998 (Pellikka *et al.* 2000, King *et al.* 2005).

The QMNR measured tree and forest structure and health parameters during the summers of 1997 and 1998. Along with tree *x*,*y* position to the nearest centimetre, forest structural variables such as diameter at breast height (DBH), tree height, vertical crown height, species and average crown size were measured for all intermediate and dominant trees. Using the known *x*,*y* position of each tree, Butson and King (1999) conducted a semivariance analysis to determine the semivariogram range for DBH, height and crown diameter and related them to the range determined from imagery of different resolutions. For the present study, as lacunarity responds to pattern scales in the imagery, only the crown size measurements were used to compare with the lacunarity curve results.

The remotely sensed data were acquired by the Ontario Ministry of Natural Resources on 18 August 1998 using a Vinten 70 mm camera with Kodak 2443 CIR film. The photographs were scanned using the Kodak Photo CD process to a nominal ground pixel size of approximately 27 cm and then re-sampled using a 2×2 averaging filter to 54 cm pixels to match the pixel size of Dataset 2 (see below). To locate the two study plots in the imagery, $2 \, m^2$ white targets were placed at open locations in the forest canopy. After image acquisition, their coordinates and the plot corner coordinates were measured using real-time differential Global Positioning System (GPS) to provide positional accuracy of about $\pm 0.5 \, m$. The images were aligned to a series of ortho-rectified photographs that the National Capital Commission (NCC) had acquired for this portion of the Gatineau Park in 1994. This image rectification process yielded an RMS error of less than two pixels. Complete ortho-rectification of the two scanned photos that contained each study plot was not considered because the study plots were relatively small within each photo and the area covered by each photo was almost flat. For lacunarity analysis, a $50 \, m \times 50 \, m$ area within each sample plot (figure 2) was extracted from the photos. As binary images were required for lacunarity derivation, the near-infrared (NIR) band was used because it had much higher contrast between canopy vegetation and gaps than did the visible bands and it is generally more sensitive to multiple scattering from understorey as well as overstorey (Treitz 2001).

3.1.2 Dataset 2. Dataset 2 consisted of six plots (numbered 1–6) of $50 \, m \times 50 \, m$ each situated on very flat topography in low land adjacent to an abandoned mine. Trembling aspen (*Populus tremuloides*) between 70 and 80 years old dominated the upper canopy with fewer numbers of white birch, black spruce (*Picea mariana*) and balsam fir (*Abies balsamea*) in the understorey. The plots were located at 40 m, 140 m, 240 m, 440 m, 640 m and 840 m from an open tailings deposit and showed variations in forest structure resulting from wind and biogeochemical stress such as acid drainage, windblown tailings deposition on trees, and high soil metal content (Lévesque and King 1999, 2003).

Field measurements included DBH, tree height, crown size, stem density, crown closure, leaf area index and a health score taken in 1993, 1995, 1997 and 1999 for the various studies at the site (see previous references). For the present study, measurements of crown size from 1999, acquired with the same methods as for Dataset 1, were used.

The remotely sensed data were collected on 20 August 1999 using a Kodak Megaplus 1.4 digital camera with 8-band filter wheel (King 1995). Nominal ground pixel size was 0.5 m. Plot location was determined using the same targets and GPS
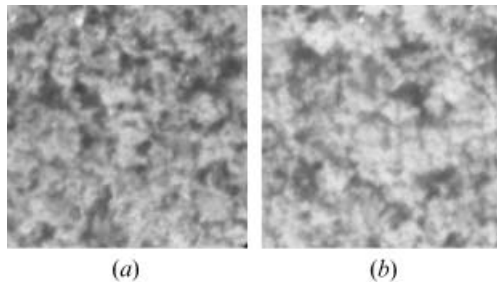

Figure 2. Dataset 1 images of plot 701 (*a*) and 702 (*b*). Nominal ground pixel size is 54 cm.

techniques as for Dataset 1. Band-to-band image registration was first performed to remove the aircraft translations between spectral bands (due to filter wheel rotation during flight). Image geo-referencing was then conducted with a model RMS error of less than one half a pixel. (More detail on the complete image acquisition and processing methodology is given in Cosmopoulos and King 2004). For lacunarity analysis, the NIR band (900 nm $\pm$ 5 nm) was used. Figure 3 shows the 50 m $\times$ 50 m image subset for each of the six plots.

3.2   *Lacunarity analysis of image data*

The 50 m $\times$ 50 m image subscenes for each plot were converted into binary images based on the mean DN value. Upper canopy trees were very bright in the images while shadows and spaces between trees were very dark. Thus, a simple threshold of the mean brightness was applied to classify tree crowns as a value of zero and shadows or spaces as a value of one (DN). Figure 4 shows the resulting binary images for Dataset 1.

   An algorithm was developed to calculate lacunarity distributions for user selected spatial extents, in this case ranging from a maximum size of 40 m $\times$ 40 m (green square in figure 4) to a minimum of 7 m $\times$ 7 m (red square in figure 4). All extents were centred about the middle pixel of the image. The 40 m extent was selected as the upper limit because it was felt that beyond this, spatial variations in site characteristics would affect forest structure variations and the resulting lacunarity calculations. The 7 m extent was selected as the lower limit since below this, image
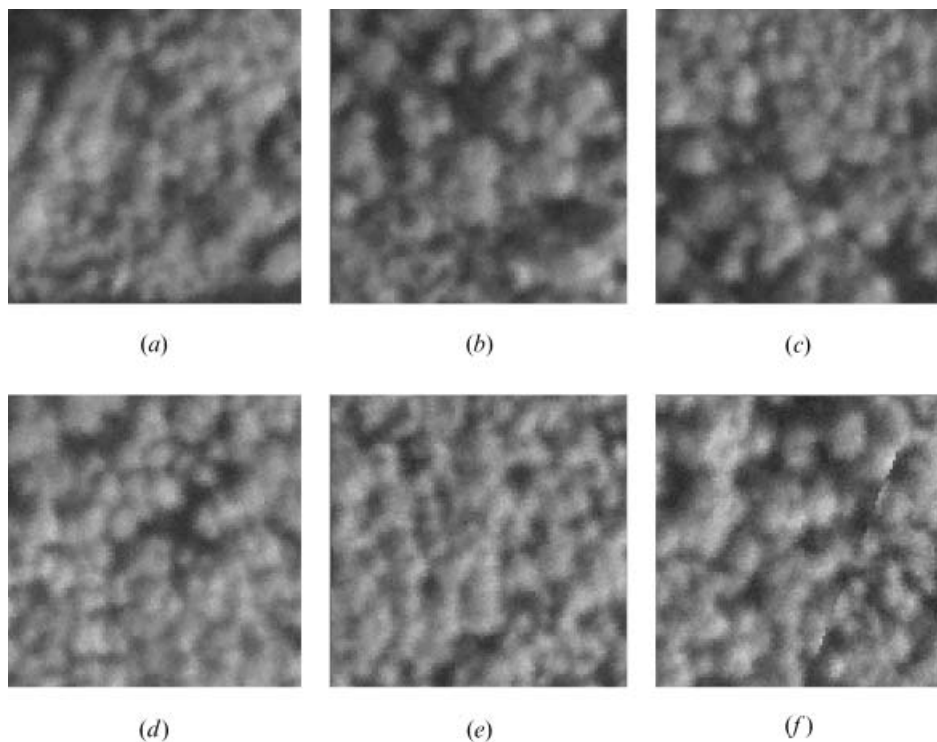

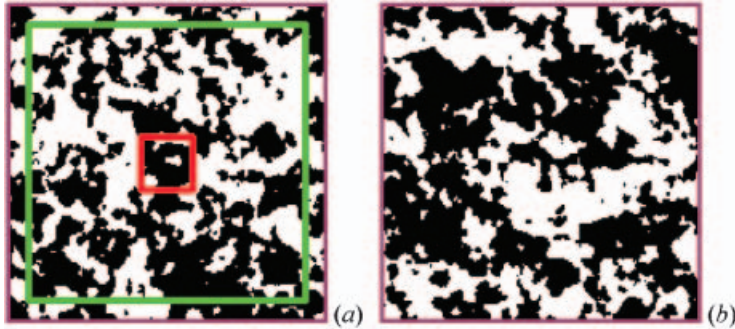Figure 3.   Dataset 2 images for plots 1–6 ((*a*)–(*f*), respectively). Nominal ground pixel size is 50 cm.

Figure 4. Binary images of plots 701 (*a*) and 702 (*b*) from Dataset 1. Tree crowns are displayed as black (0) and canopy gaps are displayed as white (1). Total spatial extent is 50 m. Lacunarity curves were generated for various extents within the range of 7 m (red square) to 40 m (green square).

spatial variability would be affected more by within crown structure. The lacunarity functions were plotted on natural log–log graphs and then converted to first-derivative slope curves similar to the example in figure 1. The form of each slope curve was interpreted for the number of troughs representing distinct pattern scales as well as for their relative width and depth. From this analysis, the optimal spatial extents were determined for each dataset.

4. Results and discussion

4.1 Dataset 1

The spatial extents and associated lacunarity analyses were separated into four groups for presentation purposes: Group 1–7, 8, 9 and 10 m; Group 2–12, 14 and 16 m; Group 3–18, 20 and 25 m; Group 4–30, 35 and 40 m.

Figure 5 shows the lacunarity slope curves for plot 701 of Dataset 1. In these curves, a deep and narrow trough indicates a distinct and discrete pattern scale while a wide trough characterizes a broader range of object sizes in the given pattern. The 8 m and 9 m extents show two pattern scales, one at 3.0 m and the other (more subtle) at 6.0 m. For the spatial extent of 7 m, the pattern scale at 3.0 m tends to dominate, while a spatial extent of 10 m does not detect any distinct patterns. The 12 m extent shows three pattern scales at 3.0 m, 6.6 m and 10.8 m (more subtle). The 14 m extent also shows three pattern scales but they are less distinct than those of the 12 m extent. Beyond the 14 m extent, the number of distinct pattern scales decreases until the overall pattern appears essentially homogeneous for extents greater than 20 m. From the graphs it is clear that the 12 m extent captures the most distinct and discrete pattern scales.

Figure 6 shows the results for plot 702. Extents of 12 m and smaller revealed one or two distinct pattern scales. The 14 m extent shows three distinct pattern scales, which are centred at 4.8 m, 9.0 m and 14.4 m. At spatial extents of 18–30 m, three scales are evident but only the 18 m extent has pattern scales close to the distinctiveness of those at 14 m. The others have wider troughs representing a broader range of object sizes present in a given pattern. For example, the third pattern scale for the 20 m extent is dominated by a dimension of 13.2 m, but objects of up to 17.4 m are influencing this pattern. At larger extents, troughs are usually wider and tend to generalize the size of objects within a pattern. Conversely, small
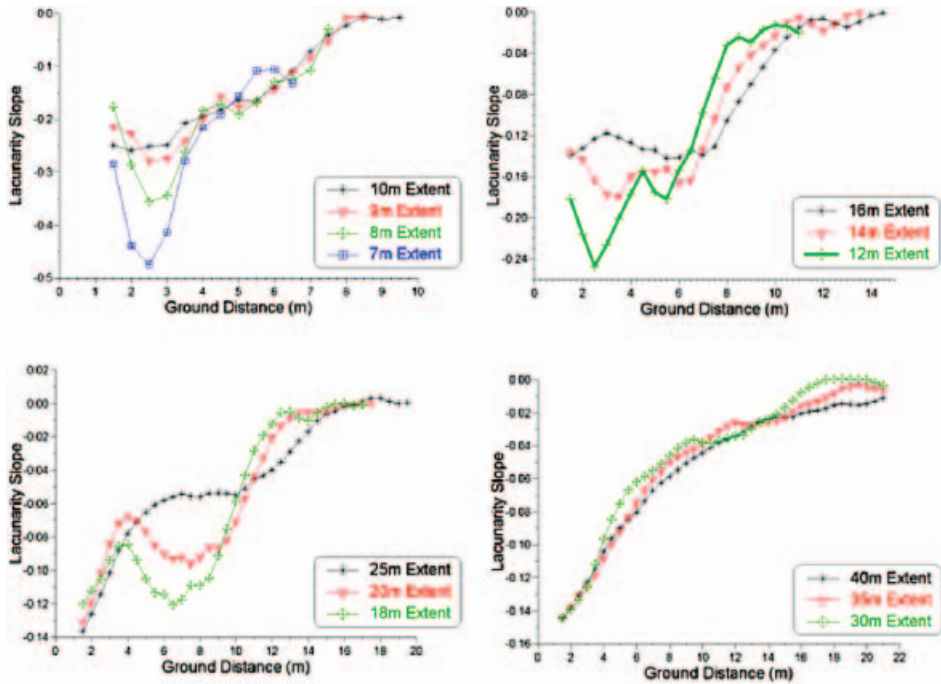
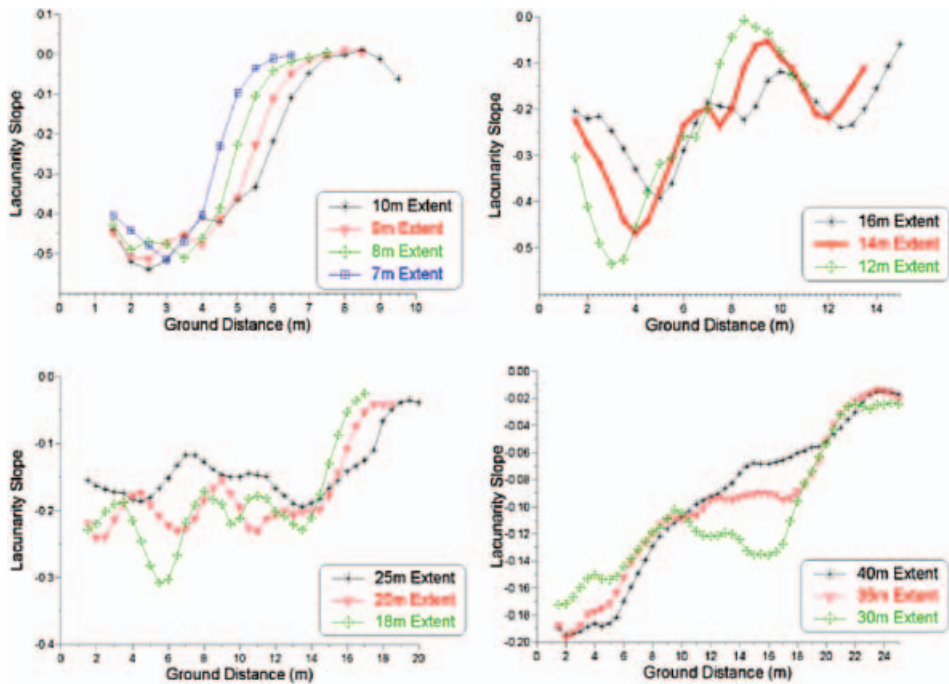Figure 5.   Lacunarity slope functions for plot 701.

Figure 6.   Lacunarity slope functions for plot 702.

extents tend to focus on specific objects that dominate the spatial pattern and measure object sizes with more specificity. Beyond the 30 m spatial extent, the number of pattern scales decreases with increasing extent until the image pattern becomes essentially homogeneous.

4.2 Dataset 2

Figure 7 shows the lacunarity slope curves for the six plots of Dataset 2. For brevity, only the curves representing the optimal spatial extent and those close to it are shown.

Following from the analysis of Dataset 1, results for Dataset 2 are presented in a more summarized manner. The optimal spatial extent is shown as the bold line in each of the lacunarity slope curves of figure 7, and the pattern scale values are given in table 1. In three of the six plots, two pattern scales were detected while in the other three plots, three were detected. The size of these patterns varied between plots due to the varied forest structure that is evident in the images of figure 3. The optimal spatial extent was between 14 m and 18 m for five of the six plots. Similar to the results for Dataset 1, extents larger than these retained fewer pattern scales or captured the same number of pattern scales but with wider ranges of object sizes in each (i.e. the pattern scales were less distinct). Spatial extents smaller than the optimum values tended to generalize the smaller scaled objects.

4.3 Relation between pattern scales and tree crown size

Table 1 shows the average field measured tree crown sizes for both datasets and the pattern scales detected by the best spatial extents in the lacunarity analyses. Intermediate crown sizes had not been measured for Dataset 2. It is evident that the scales of pattern interpreted through lacunarity analysis are linked to the primary objects in the imagery, the tree crowns, although there is some mixing between overstorey and understorey as well as partially hidden crowns. The smallest pattern scales are in the range of 2.0–4.8 m. They tended to capture the brightest pixels of the smallest dominant trees or intermediate tree crowns that were visible or partially visible to the sensor. When three pattern scales were detected, the intermediate pattern scales were in the range of 6.0–9.0 m. This most closely approximates the average dominant tree crown sizes. However, clustered and overlapping crowns result in this pattern scale being greater or less than the field measured dominant crown size depending on the degree of clustering of crowns in each plot. In addition, using the mean as a threshold to produce binary images for the lacunarity analysis may have excluded parts of the shaded sides of crowns. In future work a tree delineation algorithm that captures more of the whole crown (e.g. Pouliot *et al.* 2005) should be implemented. The largest pattern scales ranged from 5.0 m to 14.4 m. If plot 6 from Dataset 2, which had only two pattern scales, is excluded, then the range of the largest pattern scales is 7.5–14.4 m. These larger scales captured clustered and overlapping dominant crowns as well as the largest single trees in the plots.

For the six plots of Dataset 2, correlation analysis was conducted where a Pearson correlation coefficient was significant at $p \leqslant 0.05$ if it was greater than or equal to 0.81. None of the pattern scales were significantly correlated with average tree size, although the second pattern scale for each plot was close ($r=0.70$), and may have proven to be significant with more samples. These results agree with those of Dale
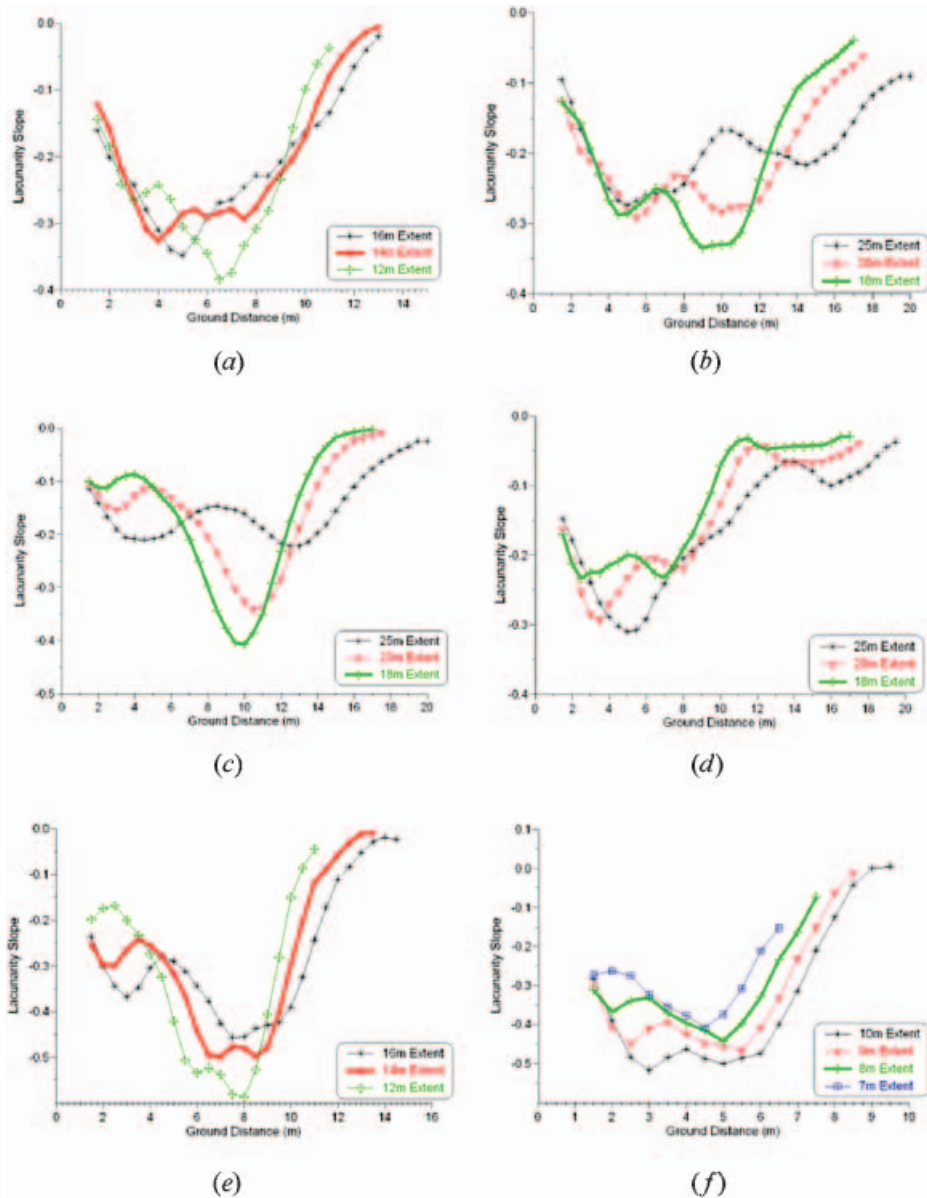
Figure 7.   Lacunarity slope curves for Dataset 2, plots 1–6 ((*a*)–(*f*), respectively).

(2000) who found for one-dimensional artificial data and measured field data that break points in the lacunarity slope curves did not correspond directly to object sizes. However, the curves derived for the image data presented here showed much more distinct pattern scales than those of Dale (2000).

   Based on the above analysis, it was concluded that the pattern scales detected in the imagery do not correspond directly to individual tree crown sizes, but are a combination of components of crowns, individual isolated crowns, and clusters of dominant and sometimes intermediate crowns.

Table 1. Image pattern scales detected by the optimal spatial extent and field measurements of tree crown diameter.

Site	Image data		Field data	
	Optimal extent (m)	Pattern scale (m)	Mean crown diameter/St. Dev. (m)	
			Dominant	Intermediate
Dataset 1				
701	12	3.0, 6.6, 10.8	7.8/2.3	5.0/1.3
702	14	4.8, 9.0, 14.4	7.2/2.2	4.9/1.4
Dataset 2				
Plot 1	14	4.0, 6.0, 7.5	5.6/1.5	–
Plot 2	18	4.5, 9.0	7.1/1.9	–
Plot 3	18	3.0, 10.0	7.2/2.1	–
Plot 4	18	2.5, 7.0, 12.5	5.8/2.0	–
Plot 5	14	2.0, 6.5, 8.5	5.1/1.5	–
Plot 6	8	2.0, 5.0	6.4/2.3	–

4.4 *Comparing lacunarity analysis to semivariogram analysis*

Geostatistical methods have also been applied in pattern analysis (e.g. Lacaze *et al.* 1994), with semivariance statistics used to specify an optimal sample extent (window size) for analysis of spatial information such as image texture (e.g. Butson and King 1999, Franklin *et al.* 2000, Treitz and Howarth 2000). It was of interest to compare the results obtained from the lacunarity analyses with those of semivariance analysis for the same data. Semivariance represents half the squared difference of a measured variable at two locations, x and $x+h$, where h is the separation (lag) between the points (Curran 1988). For a regionalized variable with measurements at more than two locations, a graph of semivariance against lag (the semivariogram) can be derived. The range of the semivariogram is the lag beyond which data points become spatially independent of each other. Lags less than the range represent the region of spatial dependence of the dataset (Curran 1988, Woodcock *et al.* 1988).

For Dataset 1, Butson and King (1999) had determined the range of the semivariogram for the same images re-sampled to 108 cm pixels to be 8.8 m for both plots 701 and 702. Repeating that analysis for the 54 cm data presented here gave ranges of 7.2 m and 8.1 m for the two plots, respectively. These values are similar to the second lacunarity pattern scales of 6.6 m for the 12 m optimal extent and 9.0 m for the 14 m optimal extent.

For Dataset 2, Lévesque and King (1999) had found the range of the 0.5 m pixel NIR band acquired in 1995 to be very highly correlated with average plot crown size, although the range values were much larger than the crown diameters (range=10.5–15.4 m). The 1995 image range was also significantly correlated ($p \leqslant 0.05$) with the average crown diameter measured in 1999 for this study ($r=0.91$) and with the second pattern scale found in the six plots ($r=0.81$). However, it was not significantly correlated with the smallest pattern scale detected ($r=0.54$), nor with the largest ($r=0.04$).

Therefore, for both datasets it is evident that the semivariance range detects the second pattern scale well, which was generally the most distinct pattern in the imagery (largest trough exhibited in the lacunarity slope curves of figures 5–7) and was directly linked to the average tree crown size. However, it did not detect the more subtle small and large pattern scales revealed in the lacunarity analysis. In

terms of the primary goal of this research to determine an optimal spatial extent for sample-based spatial image analysis (e.g. an optimal window size for image texture analysis), an extent selected as the range of the semivariogram would generally be too small to capture the larger pattern scales that were detected by lacunarity analysis. The range would indicate an optimal extent of about 8 m for Dataset 1 and 12–15 m for Dataset 2, while the lacunarity analysis indicated optimal extents of 12–14 m for Dataset 1 and 14–18 m for all but one plot in Dataset 2. Thus, for this purpose, and for development of understanding of the nature of patterns in remote sensing imagery, the capability of lacunarity analysis to detect multiple pattern scales is advantageous. These conclusions regarding the benefits of lacunarity as a multiple scale analysis method were also reached by Dale (2000) and McIntyre and Wiens (2000) for different data types.

5. Conclusions

In remote sensing studies, it is essential to know the optimal extent for image sampling or spatial analysis. Determining such an extent based on the pattern scales displayed in the imagery can be achieved using lacunarity analysis. Its capability to detect multiple pattern scales and to determine optimal spatial extents based on the number and distinctiveness of these patterns was shown to be advantageous in tests using high-resolution images from a temperate hardwood and a mixed boreal forest. The optimal spatial extent was found to be between 12 and 14 m for the temperate hardwood dataset and between 14 and 18 m for five of the six plots in the boreal dataset. For each forest, using 0.5 m pixel imagery, a sample extent equal to the upper bound of these ranges would be a conservative approach to ensure that all pattern scales present in the imagery would be captured. Alternatively, an adaptive approach using lacunarity analysis at each cell could be implemented to determine the optimal sample extents for all cells individually.

References
ALLAIN, C. and CLOITRE, M., 1991, Characterizing the lacunarity of random and deterministic fractal sets. *Physical Review*, **A44**, pp. 3552–3558.
BUTSON, C.R. and KING, D.J., 1999, Semivariance analysis of forest structure and remote sensing data to determine an optimal sample plot size. In *4th International Airborne Remote Sensing Conference and Exhibition/21st Canadian Symposium on Remote Sensing*, 21–24 June 1999, Ottawa, Ontario (Ann Arbor, MI: ERIM), vol. II, pp. 155–162.
COSMOPOULOS, Y. and KING, D.J., 2004, Temporal analysis of forest structural condition at an acid mine site using multispectral digital camera imagery. *International Journal of Remote Sensing*, **25**, pp. 2421–2440.
CURRAN, P.J., 1988, The semivariogram in remote sensing: an introduction. *Remote Sensing of Environment*, **24**, pp. 493–507.

DALE, M.R.T., 2000, Lacunarity analysis of spatial pattern: a comparison. *Landscape Ecology*, **15**, pp. 467–478.

DE COLA, L., 1989, Fractal analysis of a classified Landsat scene. *Photogrammetric Engineering and Remote Sensing*, **55**, pp. 601–610.

ELKIE, P.C. and REMPEL, R.S., 2001, Detecting scales of pattern in boreal forest landscapes. *Forest Ecology and Management*, **147**, pp. 253–261.

FRANKLIN, S.E., HALL, R.J., MOSKAL, L.M., MAUDIE, A.J. and LAVIGNE, M.B., 2000, Incorporating texture into classification of forest species composition from airborne multispectral images. *International Journal of Remote Sensing*, **21**, pp. 61–79.

GEFEN, Y., MEIR, Y., MANDELBROT, B. and AHARONY, A., 1983, Geometric implementation of hypercubic lattices with noninteger dimensionality by use of low lacunarity fractal lattices. *Physical Review Letters*, **50**, pp. 145–148.

HAY, G.J., BLASCHKE, T., MARCEAU, D.J. and BOUCHARD, A., 2003, A comparison of three image-object methods for multiscale analysis of landscape structure. *ISPRS Journal of Photogrammetry and Remote Sensing*, **57**, pp. 327–345.

HENEBRY, G.M. and KUX, H.J.H., 1995, Lacunarity as a texture measure for SAR imagery. *International Journal of Remote Sensing*, **16**, pp. 565–571.

KING, D.J., 1995, Airborne multispectral digital camera and video sensors: a critical review of system designs and applications. *Canadian Journal of Remote Sensing*, Special Issue on Aerial Optical Remote Sensing, **21**, pp. 245–273.

KING, D.J., 2002, Forest structure, health and regeneration assessment using airborne digital camera imagery. In *ForestSAT Symposium*, 5–9 August 2002, Edinburgh (Edinburgh: UK Forestry Commission, Forest Research), CD-ROM publication, 10 p.

KING, D.J., OLTHOF, I., PELLIKKA, P.K.E., SEED, E.D. and BUTSON, C., 2005, Modelling and mapping forest ice storm damage using remote sensing and environmental data. *Natural Hazards*, **35**, pp. 321–342.

LACAZE, B., RAMBAL, S. and WINKEL, T., 1994, Identifying spatial patterns of Mediterranean landscapes from geostatistical analysis of remote sensing data. *International Journal of Remote Sensing*, **15**, pp. 2437–2450.

LÉVESQUE, J. and KING, D.J., 1999, Airborne digital camera image semivariance for evaluation of forest structural damage at an acid mine site. *Remote Sensing of Environment*, **68**, pp. 112–124.

LÉVESQUE, J. and KING, D.J., 2003, Spatial analysis of radiometric fractions from high-resolution multispectral imagery for modelling forest structure and health. *Remote Sensing of Environment*, **84**, pp. 589–602.

MANDELBROT, B., 1983, *The Fractal Geometry of Nature* (New York: W.H. Freeman).

MARCEAU, D.J., HOWARTH, P.J. and GRATTON, D.J., 1994, Remote sensing and the measurement of geographical entities in a forested environment. 1. The scale and spatial aggregation problem. *Remote Sensing of Environment*, **49**, pp. 93–104.

MCGREW, J.C. Jr. and MONROE, C.B., 1993, *Statistical Problem Solving in Geography* (Dubuque, IA: Wm. C. Brown).

MCINTYRE, N.E. and WIENS, J.A., 2000, A novel use of the lacunarity index to discern landscape function. *Landscape Ecology*, **15**, pp. 313–321.

NIGH, G.D., 1997, Identifying and modeling the spatial distribution dynamics of regenerating lodgepole pine. Research Report 12, British Columbia Ministry of Forests, Forestry Division Services Branch, Victoria, BC, Canada.

PELLIKKA, P.K.E., SEED, E.D. and KING, D.J., 2000, Modelling deciduous forest ice storm damage using CIR aerial imagery and hemispheric photography. *Canadian Journal of Remote Sensing*, **26**, pp. 394–405.

PLOTNICK, R.E., GARDNER, R.H. and O'NEILL, R.V., 1993, Lacunarity indices as measures of landscape texture. *Landscape Ecology*, **8**, pp. 201–211.

PLOTNICK, R.E., GARDNER, R.H., HARGROVE, W.W., PRESTEGAARD, K. and PERLMUTTER, M., 1996, Lacunarity analysis: a general technique for the analysis of spatial patterns. *Physical Review E*, **53**, pp. 5461–5468.

POULIOT, D.A. and KING, D.J., 2005, Approaches for optimal automated individual tree crown detection in young regenerating coniferous forests. *Canadian Journal of Remote Sensing*, **31**, pp. 256–267.

POULIOT, D.A., KING, D.J. and PITT, D.G., 2005, Development and evaluation of an automated tree detection–delineation algorithm for monitoring regenerating coniferous forests. *Canadian Journal of Forest Research*, in press.

SEED, E.D. and KING, D.J., 2003, Shadow brightness and shadow fraction relations with effective LAI: importance of canopy closure and view angle in mixedwood boreal forest. *Canadian Journal of Remote Sensing*, Special Issue on Measurement and Use of Leaf Area Index in Monitoring Vegetated Ecosystems, **29**, pp. 324–335.

SIM, B.L., AGTERBERG, F.P. and BEAUDRY, C., 1999, Determining the cutoff between background and relative base metal smelter contamination levels using multi-fractal methods. *Computers and Geosciences*, **25**, pp. 1023–1041.

STITELER, W.M. and PATIL, G.P., 1971, Variance-to-mean ratio and Morisita's index as measures of spatial patterns in ecological populations. In *Statistical Ecology*, G.P. Patil, E.C. Pielou and W.E. Waters (Eds). Vol. 1, pp. 423–459 (College Town, PA: Pennsylvania State University Press).

SUN, G. and RANSON, K.J., 1998, Radar modelling of forest spatial patterns. *International Journal of Remote Sensing*, **19**, pp. 1769–1791.

TAYLOR, J.R., 1997, *An Introduction to Error Analysis* (Sausalito, CA: University Science Books).

TREITZ, P., 2001, Variogram analysis of high spatial resolution remote sensing data: an examination of boreal forest ecosystems. *International Journal of Remote Sensing*, **22**, pp. 3895–3900.

TREITZ, P. and HOWARTH, P.J., 2000, High spatial resolution remote sensing data for forest ecosystem classification: an examination of spatial scale. *Remote Sensing of Environment*, **72**, pp. 268–289.

UPTON, G.J.G. and FINGLETON, B., 1985, *Spatial Data Analysis by Example*, Vol. 1 (Toronto: John Wiley).

WEISHAMPEL, J.F., SLOAN, J.H., BOUTET, J.C. and GODIN, J.R., 1998, Mesoscale changes in textural pattern of 'intact' Peruvian rainforests (1970's–1980's). *International Journal of Remote Sensing*, **19**, pp. 1007–1014.

WITH, K.A. and KING, A.W., 1999, Dispersal success on fractal landscapes: a consequence of lacunarity thresholds. *Landscape Ecology*, **14**, pp. 73–82.

WOODCOCK, C.E. and STRAHLER, A.H., 1987, The factor of scale in remote sensing. *Remote Sensing of Environment*, **21**, pp. 311–332.

WOODCOCK, C.E., STRAHLER, A.H. and JUPP, D.B., 1988, The use of variograms in remote sensing: I. Scene models and simulated images. *Remote Sensing of Environment*, **25**, pp. 323–348.

ZOLADESKI, C.A. and MAYCOCK, P.F., 1990, Dynamics of the boreal forest in Northwestern Ontario. *The American Midland Naturalist*, **124**, pp. 289–300.